Demonstration of Al:ZnO as a plasmonic component for near-infrared metamaterials

Gururaj V. Naik[a], Jingjing Liu[a], Alexander V. Kildishev[a], Vladimir M. Shalaev[a,b], and Alexandra Boltasseva[a,c,1]

[a]School of Electrical and Computer Engineering, and Birck Nanotechnology Center, Purdue University, West Lafayette, IN 47907; [b]The Russian Quantum Center, Moscow 119991, Russia; and [c]DTU Fotonik, Technical University of Denmark, Lyngby 2800, Denmark

Edited by* Federico Capasso, Harvard University, Cambridge, MA, and approved March 26, 2012 (received for review December 30, 2011)

Noble metals such as gold and silver are conventionally used as the primary plasmonic building blocks of optical metamaterials. Making subwavelength-scale structural elements from these metals not only seriously limits the optical performance of a device due to high absorption, it also substantially complicates the manufacturing process of nearly all metamaterial devices in the optical wavelength range. As an alternative to noble metals, we propose to use heavily doped oxide semiconductors that offer both functional and fabrication advantages in the near-infrared wavelength range. In this letter, we replace a metal with aluminum-doped zinc oxide as a new plasmonic material and experimentally demonstrate negative refraction in an Al:ZnO/ZnO metamaterial in the near-infrared range.

transparent conducting oxides | heavily doped semiconductors | low-loss metals

The recent emergence of plasmonics (1, 2) and metamaterials (3) has led to the demonstration of optical devices with many unconventional functionalities such as subdiffraction imaging (4, 5), cloaking (6), and optical magnetism (7). These novel functionalities have been demonstrated through exciting proof-of-principle experiments performed in the ultraviolet (UV), infrared (IR), or microwave frequency ranges (4–6, 8). The experimental demonstrations of similar devices in the visible and near-IR ranges would have a significantly larger impact owing to the technological importance of these frequency ranges. However, the major problem impeding the realization of efficient devices in these important spectral ranges is the optical loss associated with the metallic constituents in metamaterial building blocks (9–11). The development of new constituent materials for low-loss, metamaterial-based devices is therefore required for realistic applications of metamaterials in the visible and near-IR (10, 12, 13). Previously, we reported that heavily doped oxide semiconductors like transparent conducting oxides could serve as good alternatives to metals for the realization of many classes of metamaterials, including metamaterials with hyperbolic dispersion (14, 15) in the near-IR (16). Here, we have designed, fabricated, and characterized a nonresonant, plasmonic, metamaterial device in which the noble metal acting as the constituent plasmonic building block has been replaced by aluminum-doped zinc oxide (Al:ZnO, herein referred to as AZO). As a proof-of-concept demonstration, we experimentally show that, similar to traditional metal-dielectric structures, a device built of alternating subwavelength AZO/ZnO layers exhibits negative refraction in the near-IR range. We also show that the performance of the AZO/ZnO device is significantly better than that of conventional metal-based devices.

Optical metamaterials typically use nanostructured metals and dielectrics as their building blocks. The geometry of the unit cell and the optical properties of the constituent materials form the parameter space for the device design. In the near-IR and shorter wavelength ranges, the geometry is restricted by nanofabrication capabilities since unit cells cannot be made arbitrarily small. Thus, the optical properties of the constituent natural materials form an important set of design parameters. The optical properties of bulk natural materials are described only by their complex-valued and dispersive permittivities or dielectric functions (ε), as their permeabilities are unity at optical frequencies. The real part of the dielectric function (ε' or $\mathrm{Re}(\varepsilon)$) signifies the electrical polarization response of the material, while the imaginary part (ε'' or $\mathrm{Im}(\varepsilon)$) describes the material losses. When designing a low-loss, high-performance metamaterial, one can choose dielectric materials (for an $\varepsilon' > 0$ contribution) having negligible losses. However, metals that offer negative real permittivity ($\varepsilon' < 0$) exhibit strong optical dispersion, which is accompanied by large losses. Even noble metals like silver and gold (the metals with the highest DC conductivities) exhibit excessive losses at optical frequencies that seriously restrict the experimental realization of metamaterial devices in the optical frequency range. Furthermore, for noble metals, the real part of their permittivity is very large in magnitude. Due to the fact that many devices based on transformation optics (TO) (17) require the polarization responses of the metallic and dielectric constituents to be nearly balanced (18), the extreme contrast in magnitude between the negative (metallic) and positive (dielectric) real parts of the constituent permittivities could cause additional problems in the fabrication of metamaterial devices. The robust fabrication of balanced TO structures requires that the volume fractions of the metal and dielectric components are comparable along with comparable magnitudes of the real parts of their dielectric functions. At optical frequencies, ε' of dielectrics is on the order of 1 to 10 (e.g., ε' of Al_2O_3 is about 3 at 1.5 μm), while ε' of noble metals is about one or even two orders higher (−115 for Ag at 1.5 μm). Such a large magnitude discrepancy necessitates that the geometrical scale of the subwavelength metallic elements should be up to 100 times smaller than the dimensions of the dielectric elements (18–20), which can pose severe fabrication challenges. Another significant drawback when working with conventional metals like Au and Ag is that their optical properties are not tunable and cannot be adjusted to fit the requirements of a specific metamaterial design. An even worse disadvantage of using traditional metals for metamaterial devices and their applications is the issue of compatibility and integration: The processing of noble metals is not compatible with standard silicon nanofabrication technology. This fabrication incompatibility precludes the integration of plasmonic structures and metamaterials with nanoelectronics; hence, this is a serious threat to the development of real-life metamaterial applications. In contrast, alternative plasmonic materials such as heavily doped semiconductors provide adjustability through doping properties and lower optical loss combined with well-established fabrication methods and straightforward integration into complex device geometries.

Author contributions: G.V.N., V.M.S., and A.B. designed research; G.V.N. and J.L. performed research; G.V.N., J.L., A.V.K., and A.B. analyzed data; G.V.N., J.L., A.V.K., V.M.S., and A.B. wrote the paper.

The authors declare no conflict of interest.

*This Direct Submission article had a prearranged editor.

[1]To whom correspondence should be addressed. E-mail: aeb@purdue.edu.

This article contains supporting information online at www.pnas.org/lookup/suppl/doi:10.1073/pnas.1121517109/-/DCSupplemental.

Heavily Doped Semiconductors

Semiconductors offer great tunability in their properties (e.g., by doping). Conventional semiconductors like GaAs or ZnO are dielectrics in the optical range and, hence, their use in plasmonics and optical metamaterials has so far been limited to providing a dielectric background. Being very attractive materials due to their optical properties and tunability, semiconductors have long been the subject of a great deal of attention in the materials community. It was an important development for the metamaterial field to demonstrate that heavy doping can make semiconductors exhibit metal-like properties in the mid-IR (21). However, the typically used doping levels of about 10^{18} to 10^{19} cm^{-3} cannot make semiconductors exhibit metallic properties in the near-IR, and even higher doping ($\sim 10^{21}$ cm^{-3}) is required to make semiconductors metallic at these optical frequencies. Such ultrahigh doping in semiconductors poses significant challenges because of solid-solubility limits (22, 23) and low dopant ionization efficiencies (24). A solution to these issues can be offered by oxide semiconductors that allow ultrahigh doping as a result of their higher solid-solubility limits (25) and hence could exhibit metallic properties in the near-IR. Heavily doped zinc oxide, one of a family of transparent conducting oxides (TCOs), is a highly conducting material that has been used in applications such as liquid-crystal displays. Zinc oxide can be heavily doped ($\sim 10^{21}$ cm^{-3}) by trivalent dopants such as aluminum and gallium (22, 23). Ultrahigh doping results in a large carrier concentration (10^{20} to 10^{21} cm^{-3}), which enables Drude metal-like optical properties in the near-IR and leads to negative values of the real part of permittivity for doped zinc oxide and other TCOs (26). While the carrier concentration is related to the metallic properties of TCO films, the carrier relaxation rate or Drude damping relates to the optical losses in TCO films (27). Since losses are detrimental to the performance of devices (10), Drude damping must be kept as low as possible in these materials. Previously, we studied various TCOs and found that AZO exhibits the lowest losses, about five times lower than the loss in silver in the near-IR, owing to its small Drude-damping coefficient (10, 13). In this report, we demonstrate a high-performance hyperbolic metamaterial (HMM) formed by AZO and ZnO as the metallic and dielectric components, respectively, and show proof-of-principle results using this device in a well-known negative refraction experiment.

Negative Refraction Experiment

A uniaxial material that has different signs of real permittivity in different directions is a HMM (14, 15). Consequently, there are two possibilities for this to occur: The real permittivity parallel to the uniaxial crystal planes is positive ($\varepsilon_{\parallel} > 0$) and that perpendicular to the planes is negative ($\varepsilon_{\perp} < 0$), herein referred to as a transverse-positive HMM; or $\varepsilon_{\parallel} < 0$ and $\varepsilon_{\perp} > 0$, which we label as a transverse-negative HMM. It is only the transverse-positive HMM that can exhibit negative refraction or hyperlensing (4, 21, 28–30). Such applications are enabled by realizing hyperbolic dispersion in metal-dielectric composite structures. Subwavelength building blocks of metallic and dielectric components could exhibit the desired uniaxial anisotropy in the effective-medium limit (14, 31). Two types of design are used in HMMs: A planar design consisting of alternating layers of metal and dielectric (21, 32), and metal nanowires embedded in a dielectric medium (29, 30). The planar design has many advantages over the nanowire structure because its fabrication is simple and robust. Moreover, it can be easily integrated with other components into more complex device geometries using standard, planar fabrication processes. However, achieving transverse-positive hyperbolic dispersion in a planar structure is very challenging, especially in the near-IR and visible ranges. This is because metals that are typically used to build such a planar metamaterial have a very large magnitude of the real part of their dielectric permittivity. In other words, conventional metals such as silver and gold are too metallic to be useful as building blocks for a hyperlens or a negatively refracting slab in the near-IR. On the other hand, ultrahighly doped semiconductors such as ZnO behave as "mild" or diluted metals in the near-IR, which can enable high-performance HMM-based devices. Furthermore, a material system such as ZnO and AZO has an evident advantage from the perspective of material technology: These materials allow the epitaxial, superlattice design of the device structure, which can reduce the losses at the layer interfaces and thus further boost the device performance.

In our experiments, the planar HMM was formed by depositing 16 alternating layers of AZO and ZnO, each about 60 nm thick, on a silicon substrate. The deposition was carried out using laser ablation of Al_2O_3 : ZnO (2 weight %) and ZnO targets. High purity, sintered, and pressed targets were purchased from K. J. Lesker with purity of at least 99.999%. The deposition conditions of AZO were optimized previously to produce a low-loss plasmonic material (16). The AZO/ZnO planar HMM was characterized using spectroscopic ellipsometer (V-VASE, J. A. Woollam Co.). The optical constants of the individual layers were extracted using a Drude + Lorentz model for AZO and a Lorentz model for ZnO. The models were chosen to describe the optical phenomena occurring in these materials in the wavelength range of interest. While the Lorentz model is used to describe the onset of interband transitions in ZnO in the ultraviolet, the Drude model is used to capture the free-electron response to the optical field (33). Fig. 1*A* shows dielectric functions of AZO and ZnO thin films retrieved from ellipsometric measurements. In the near-IR range, AZO shows negative real permittivity for wavelengths longer than 1.84 μm, which allows AZO to be a metal substitute in the HMM design. The metallic properties of AZO in the longer wavelength range follow the Drude model, which may be used to estimate the carrier concentration in the fabricated films. The carrier concentration in the manufactured AZO films was estimated to be approximately 4.3×10^{20} cm^{-3}. Zinc oxide is a lossless dielectric with real permittivity close to 4 in the near-IR range. An alternating multilayer stack of AZO and ZnO with each elemental layer thickness (60 nm) being a small fraction (e.g., 1/30) of the wavelength can be approximated as a uniaxial medium in the effective-medium limit (see *Supporting Information* and Fig. S1 for more details on effective medium theory). The layered stack exhibits different permittivity values in the plane parallel to the layers and the direction perpendicular to the layers. The effective optical properties in these two directions were extracted from the ellipsometry data using a uniaxial model. Fig. 1*B* shows the effective dielectric functions in the plane parallel to the layers ($\varepsilon_{\parallel}$) and

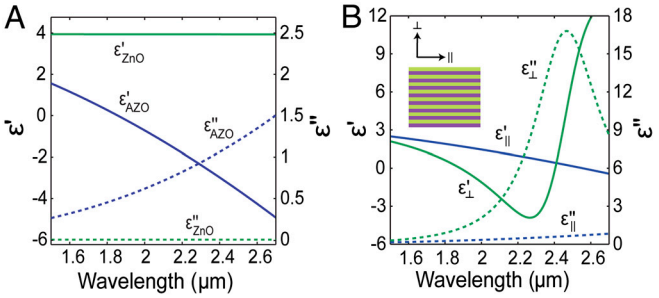

Fig. 1. Optical properties extracted from ellipsometry measurements. (*A*) Dielectric functions of ZnO and Al-doped ZnO (AZO) in the near-IR. AZO is metallic for wavelengths longer than 1.84 μm. (*B*) Dielectric functions of an alternating-layer stack of AZO and ZnO thin films (the inset shows the schematic of the layer stack) retrieved using a uniaxial model. The real and imaginary parts of permittivity in the plane parallel to the layers (represented as ∥) and perpendicular to the layers (represented as ⊥) are plotted in the near-IR. In the wavelength range from 1.84 μm to 2.4 μm, the layer stack shows transverse-positive ($\mathrm{Re}(\varepsilon_{\parallel}) > 0$, $\mathrm{Re}(\varepsilon_{\perp}) < 0$) hyperbolic dispersion. For longer wavelengths, the layer stack exhibits transverse-negative ($\mathrm{Re}(\varepsilon_{\parallel}) < 0$, $\mathrm{Re}(\varepsilon_{\perp}) > 0$) hyperbolic dispersion.

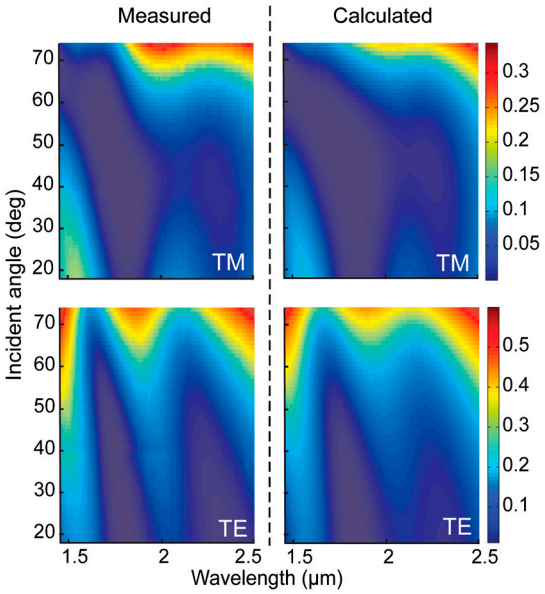

Fig. 2. Reflectance color maps of the layer stack sample in TM and TE polarizations for angles of incidence from 18 to 74 degrees. The left panels plot the measured reflectance spectra, and the right panels plot the calculated reflectance spectra in both TM and TE polarizations.

in the direction perpendicular to the layers ($\varepsilon_\perp$). For wavelengths longer than 1.84 μm, the signs of the real permittivity components in the two different directions are opposite to each other, and therefore the material exhibits hyperbolic dispersion in this range. In the wavelength range from 1.84 μm to 2.4 μm, the multilayer stack exhibits transverse-positive hyperbolic dispersion ($\mathrm{Re}(\varepsilon_\parallel) > 0$ and $\mathrm{Re}(\varepsilon_\perp) < 0$). Since transverse-positive dispersion is essential for the phenomenon of negative refraction, we could expect this planar device to refract "negatively" in the wavelength range from 1.84 μm to 2.4 μm. Note that for wavelengths longer than 2.4 μm, the multilayer stack shows transverse-negative hyperbolic dispersion.

The ellipsometry extraction of the optical parameters of the layered structure was verified by measuring far-field reflectance and transmittance in both transverse-magnetic (TM) and transverse-electric (TE) modes. The measurements were carried out at various angles of incidence ranging from 18 to 74 °. The measured reflectance spectra are plotted as color maps in the left panel of Fig. 2 for both incident polarizations. In comparison to the measured reflectance, the right panel of Fig. 2 plots the

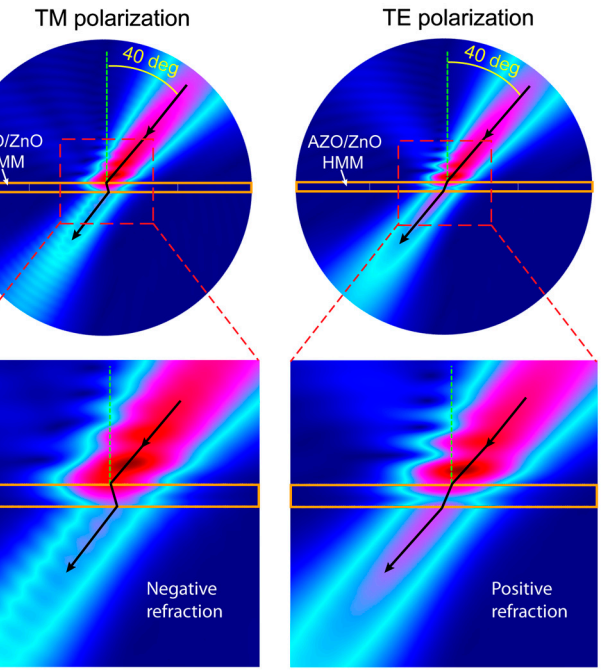

Fig. 3. Field maps showing the interaction of electromagnetic wave with AZO /ZnO multilayer stack. The incident Gaussian beam is TM polarized in the left panels and TE polarized in the right panels. The wavelength of the incident beam is 2 μm, and the angle of incidence is 40 degrees. The position of the AZO /ZnO multilayer stack is indicated by the orange rectangle. The bottom panels are the zoomed-in views of the top panels. The TM-polarization case exhibits negative refraction with respect to the sample normal and produces a significant beam shift to the incident side of the sample normal. In contrast with the TM case, the TE-polarized light is refracted positively and hence does not produce similar beam shift.

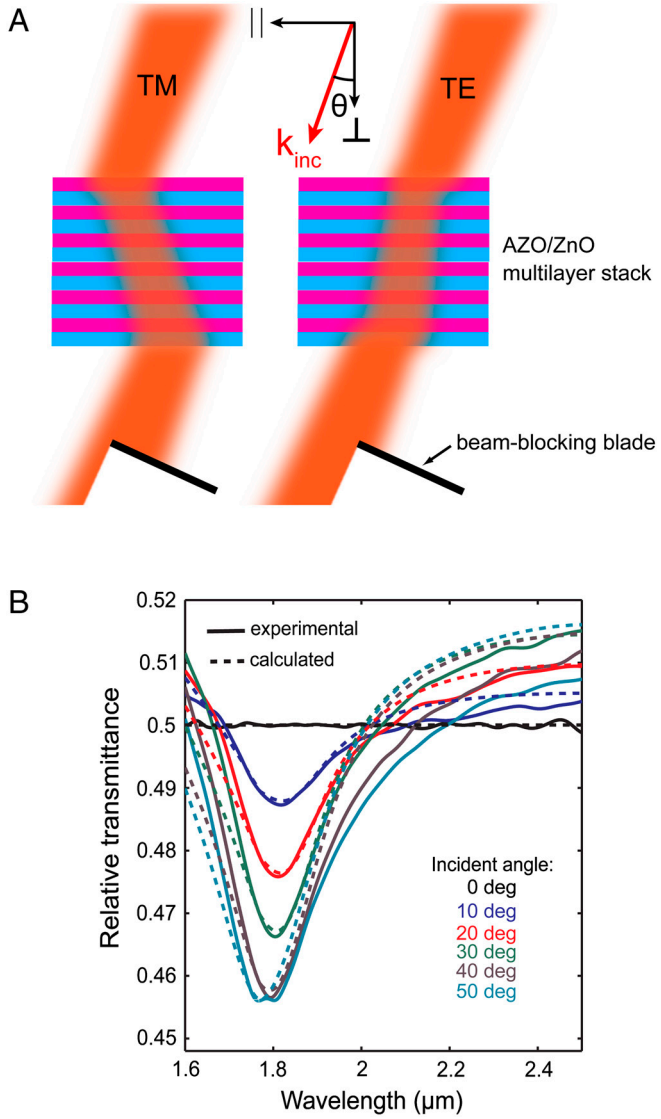

Fig. 4. Observation of negative refraction: (*A*) Schematic showing the experiemental setup for the measurement of negative refraction. The transmitted beam is blocked partially by a razor blade before it reaches the detector. In the TM case, the incident beam undergoes negative refraction and gets blocked more by the blade resulting in lower transmittance. In the TE case, the incident beam undergoes positive refraction and gets less blocked by the balde resulting in higher tranmittance. (*B*) Relative transmittance (ratio of transmittance with and without a blade partially blocking the beam) for different angles of incidence from 0 to 50 degrees. The solid curves are the measured values, and the dashed curves are calculated from theory. The dip in the relative transmittance provides evidence of negative refraction in the case of TM polarization.

calculated reflectance spectra (34) for the multilayer stack. The calculations use material properties extracted from ellipsometer measurements, as shown in Fig. 1*A*. The reflectance spectra from measurements and calculations are in good agreement, confirming the correctness of the ellipsometric extraction procedure for the optical parameters. The transmittance plots can be found in the supplementary information (Fig. S2).

In order to visualize negative refraction in the wavelength range from 1.84 μm to 2.4 μm in the fabricated slab, simulations were carried out using the extracted material parameters for AZO and ZnO. The field maps of the simulations in TM and TE polarizations are shown in Fig. 3. The TM-polarized Gaussian beam incident at an angle of 40 ° to the sample normal undergoes negative refraction inside the sample, producing a beam shift toward the incident side of the sample normal. This dramatic effect is observed only in the case of TM-polarized (*p*-polarized) incident light because only in this polarization is the electric field component of the incident light able to probe both components of the dielectric function and thus experience the material's hyperbolic dispersion. In the case of TE-polarized (*s*-polarized) incident light, the medium behaves as an isotropic dielectric with a real permittivity given by $\varepsilon_{\|}$. Since observing the anomalous beam shift in the TM case would provide evidence for negative refraction, transmittance measurements were performed on the multilayer stack with half of the transmitted beam blocked by a razor blade. Fig. 4*A* shows the schematic of the experimental setup for observing negative refraction in our ZnO-based HMM. The details of the experimental set-up are shown in *SI Text*, Fig. S3. The position of the razor blade was adjusted to block the transmitted beam intensity exactly at 50% at normal incidence. We then increased the incidence angle and recorded the beam shift by measuring the relative transmittance (ratio of transmittance with and without the blade). It may be noted from Fig. 4*A* that the relative transmittance should dip if negative refraction were to occur. Fig. 4*B* plots the ratio of the transmittance with and without the beam-blocking blade (referred to as "relative transmittance"). The figure also compares the measured curves with the theoretically predicted results. The theoretical predictions were carried out using the exact dispersion equation for a bulk, planar, multilayer stack (31) (see Fig. S1). The relative transmittance dips around 1.8 μm wavelength in the TM polarization due to negative refraction. No similar dip in the relative transmittance is observed for any incident angle in the TE-polarization (see Fig. S4). The theoretical predictions agree well with the experiments, thus confirming our observation of negative refraction in the AZO/ZnO metamaterial.

The performance of HMMs can be characterized by a figure of merit (FoM). For a negatively refracting slab such as the device in this work, Hoffman et al. introduced the FoM as (21): $\mathrm{FoM} = \mathrm{Re}(\beta_{\perp})/\mathrm{Im}(\beta_{\perp})$, where $\beta_{\perp}$ is the propagation vector in the direction perpendicular to the layers. A large FoM requires smaller $\mathrm{Im}(\beta_{\perp})$ (i.e., lower losses) and larger $\mathrm{Re}(\beta_{\perp})$ (i.e., higher effective index). The FoM for our AZO/ZnO HMM was found to be about 12, which is at least three orders of magnitude larger than that of HMMs with a similar design using silver or gold (35). In fact, the FoM in our sample is the highest FoM achieved so far in the optical range for any negatively refracting HMM (4, 29). This conclusively shows that ultrahighly doped semiconductors can serve as good alternatives to metals for certain metamaterial applications in the near-IR.

Conclusions

In summary, we designed and fabricated a semiconductor hyperbolic metamaterial in the near-IR and in which AZO replaced conventional metals. Using the AZO/ZnO metamaterial, we successfully demonstrated negative refraction in the near-IR and showed that the figure of merit of this multilayered stack is about three orders of magnitude larger than that of its metal-based counterpart.

Furthermore, alternative plasmonic materials such as AZO overcome the bottleneck created by conventional metals in the design of optical metamaterials and enable more efficient devices. This demonstration opens up approaches to engineer optical metamaterials and customizes their optical properties in order to develop optical devices with enhanced performance. We anticipate that the development of new plasmonic materials and nanostructured material composites such as AZO/ZnO will lead to tremendous progress in the technology of optical metamaterials, enabling the full-scale development of this technology and uncovering many new physical phenomena.

ACKNOWLEDGMENTS. This work was supported in part by the Office of Naval Research Grant N00014-10-1-0942, the Army Research Office Grants W911NF-04-1-0350, 50342-PH-MUR, W911NF-11-1-0359, Air Force Office of Scientific Research Grant FA9550-10-1-0264, and National Science Foundation Grant DMR-1120923. A.V.K. was supported by the Air Force Research Laboratory–Materials and Manufacturing Directorate Applied Metamaterials Program with helpful assistance by UES, Inc.

1. Maier SA (2007) *Plasmonics: Fundamentals and Applications* (Springer, New York).
2. Lal S, Link S, Halas NJ (2007) Nano-optics from sensing to waveguiding. *Nat Photonics* 1 (11):641–648.
3. Smith D, Pendry J, Wiltshire M (2004) Metamaterials and negative refractive index. *Science* 305(5685):788–792.
4. Liu Z, Lee H, Xiong Y, Sun C, Zhang X (2007) Far-field optical hyperlens magnifying sub-diffraction-limited objects. *Science* 315(5819):1686.
5. Fang N, Lee H, Sun C, Zhang X (2005) Sub-diffraction-limited optical imaging with a silver superlens. *Science* 308(5721):534–537.
6. Schurig D, et al. (2006) Metamaterial electromagnetic cloak at microwave frequencies. *Science* 314(5801):977–980.
7. Soukoulis CM, Linden S, Wegener M (2007) Negative refractive index at optical wavelengths. *Science* 315(5808):47–49.
8. Kehr SC, et al. (2011) Near-field examination of perovskite-based superlenses and superlens-enhanced probe-object coupling. *Nat Commun* 2:249.
9. Boltasseva A, Atwater HA (2011) Low-loss plasmonic metamaterials. *Science* 331 (6015):290–291.
10. West P, et al. (2010) Searching for better plasmonic materials. *Laser Photon Rev* 4(6):795–808.
11. Khurgin JB, Sun G (2010) In search of the elusive lossless metal. *Appl Phys Lett* 96(18):181102.
12. Noginov M, et al. (2011) Transparent conductive oxides: plasmonic materials for telecom wavelengths. *Appl Phys Lett* 99:021101.
13. Frölich A, Wegener M (2011) Spectroscopic characterization of highly doped ZnO films grown by atomic-layer deposition for three-dimensional infrared metamaterials [Invited]. *Opt Mater Express* 1(5):883–889.
14. Podolskiy VA, Narimanov EE (2005) Strongly anisotropic waveguide as a nonmagnetic left-handed system. *Phys Rev B* 71(20):201101.
15. Jacob Z, Alekseyev LV, Narimanov E (2006) Optical hyperlens: Far-field imaging beyond the diffraction limit. *Opt Express* 14(18):8247–8256.
16. Naik G, Boltasseva A (2010) Semiconductors for plasmonics and metamaterials. *Physica Status Solidi RRL: Rapid Research Letters* 4:295–297.
17. Pendry JB, Schurig D, Smith DR (2006) Controlling electromagnetic fields. *Science* 312(5781):1780–1782.
18. Kildishev A, Shalaev V (2008) Engineering space for light via transformation optics. *Opt Lett* 33(1):43–45.
19. Yagil Y, Deutscher G (1987) Transmittance of thin metal films near the percolation threshold. *Thin Solid Films* 152(3):465–471.
20. McCarthy S (1976) Optical properties of ultrathin Ag films. *J Vac Sci Technol* 13(1): 135–138.
21. Hoffman A, et al. (2007) Negative refraction in semiconductor metamaterials. *Nat Mater* 6(12):946–950.
22. Panish M, Casey H, Jr (1967) The solid solubility limits of zinc in GaAs at 1000. *J Phys Chem Solids* 28(9):1673–1684.
23. Neave J, Dobson P, Harris J, Dawson P, Joyce B (1983) Silicon doping of MBE-grown GaAs films. *Appl Phys A: Mat Sci Process* 32(4):195–200.
24. Wolfe C, Stillman G (1975) Self-compensation of donors in high purity GaAs. *Appl Phys Lett* 27(10):564–567.
25. Yoon M, Lee S, Park H, Kim H, Jang M (2002) Solid solubility limits of Ga and Al in ZnO. *J Mater Sci Lett* 21(21):1703–1704.
26. Naik GV, Kim J, Boltasseva A (2011) Oxides and nitrides as alternative plasmonic materials in the optical range [Invited]. *Opt Mater Express* 1(6):1090–1099.
27. Ashcroft NW, Mermin ND (1976) *Solid State Physics*, (Saunders College, Philadelphia), 1, pp 16–20.
28. Lindell IV, Tretyakov S, Nikoskinen K, Ilvonen S (2001) BW media—media with negative parameters, capable of supporting backward waves. *Microw Opt Technol Lett* 31(2):129–133.
29. Yao J, et al. (2008) Optical negative refraction in bulk metamaterials of nanowires. *Science* 321(5891):930.

30. Noginov M, et al. (2009) Bulk photonic metamaterial with hyperbolic dispersion. *Appl Phys Lett* 94:151105.
31. Rytov SM (1956) Electromagnetic properties of a finely stratified medium. *Sov Phys JETP* 2:466–475.
32. Jacob Z, et al. (2010) Engineering photonic density of states using metamaterials. *Appl Phys B Lasers and Optics* 100:215–218.
33. Oates TWH, Ranjan M, Facsko S, Arwin H (2011) Highly anisotropic effective dielectric functions of silver nanoparticle arrays. *Opt Express* 19(3):2014–2028.
34. Kildishev AV, Chettiar U (2007) Cascading optical negative index metamaterials. *Applied Computational Electromagnetics Society Journal* 22(1):172.
35. Naik GV, Boltasseva A (2011) A comparative study of semiconductor-based plasmonic metamaterials. *Metamaterials* 5(1):1–7.